communications
earth & environment

ARTICLE

https://doi.org/10.1038/s43247-022-00611-6 OPEN

Himalayan zircons resurface in Sumatran arc volcanoes through sediment recycling

Meng-Hao Gao[1], Ping-Ping Liu [1✉], Sun-Lin Chung [2,3], Qiu-Li Li [4], Bin Wang[1], Wei Tian[1], Xian-Hua Li [4] & Hao-Yang Lee[2]

Understanding the processes of subducted sediment recycling in subduction zones is vital to decipher Earth's crust-mantle interactions. This study uses along-arc geochemical variations and zircon U-Pb-Hf-O isotopes of Quaternary arc basalts and andesites on Sumatra Island, Indonesia to assess the mode of sediment recycling in subduction zones. The Hf-O isotopes of inherited zircons of the basalts and andesites near the Toba Caldera indicate that some of them were derived from subducted terrigenous sediments mainly sourced from the (eastern) Himalaya. Hybridization of the subducted sediments with the mantle also accounts for the enriched Sr-Nd isotopic compositions of arc volcanic rocks near the Toba Caldera. Thermodynamic modeling indicates that the subducted sediments did not melt on the slab surface. Rather, geochemical evidence supports their formation as diapirs that rise buoyantly through the hot mantle wedge and contribute to ~30 to 45% of the magma source of the arc volcanic rocks near Toba.

[1] Key Laboratory of Orogenic Belts and Crustal Evolution, School of Earth and Space Sciences, Peking University, Beijing, China. [2] Institute of Earth Sciences, Academia Sinica, Taipei, Taiwan. [3] Department of Geosciences, National Taiwan University, Taipei, Taiwan. [4] Institute of Geology and Geophysics, Chinese Academy of Sciences, Beijing, China. ✉email: ppliu@pku.edu.cn

Subducted sediments are indispensable components of the subduction factory. The fate of the subducted sediments has fundamental controls on mantle heterogeneity and geochemistry of arc magmas[1–5]. Identification of the contribution of subducted sediments to volcanic rocks on continental arcs is much more complicated than those on island arcs due to the possibility of contamination of the silicic upper continental crust, which shares a similar composition with the mean of the subducted sediments[3,6]. Moreover, the thermal models of the participation of subducted sediments in arc volcanic systems have been controversial. Some argue that the temperature conditions of the subducting plate at subarc depths are far below the sediments' solidus, such that the sediments mainly undergo dehydration and release fluids rich in Rb, Cs, Ba, and Pb ($D^{fluid/solid} \geq 10$), leading to flux melting of the mantle wedge[7,8]. Alternatively, it has been suggested that melting of the subducted sediments may occur at subarc depths[9]. Whether the sediments melt on the subducting slab-mantle wedge interface or during their ascent through the mantle wedge as buoyantly upwelling diapirs is unclear[10–14].

The volcanic rocks on the Sunda arc have a wide range of Sr, Nd, and Pb isotopic compositions, e.g., $^{87}Sr/^{86}Sr = 0.704$ to 0.714[15]. In particular, arc volcanic rocks near the Toba Caldera have significantly more enriched Sr and Nd isotopic compositions than those away from it[15–17]. An assimilation-fractional crystallization (AFC) model has indicated that the enriched Sr isotopic signature of arc volcanic rocks near Toba is produced by fractional crystallization of a primitive basaltic parental magma accompanied by assimilation of the most Sr isotope-enriched granite ($^{87}Sr/^{86}Sr = 0.74036$) on Sumatra[16]. However, this granite has an ε_{Nd} value of −8.35, significantly higher than the basaltic lava ($\varepsilon_{Nd} = -9.87$ to -9.62)[16,18], inconsistent with the AFC model. An alternative hypothesis is that the enriched Sr and Nd isotopes were due to the addition of the subducted sediments[15]. Thus, the along-arc geochemical variations of the Sumatran volcanic rocks are natural laboratories to investigate the contribution and behavior of subducted sediments.

In this study, we carried out systematic analyses of whole-rock geochemical compositions, in situ Sr isotopes of plagioclase phenocrysts, and U-Pb-Hf-O isotopes of inherited zircons from basalts and andesites along the Sunda arc in northern Sumatra. Through comparison of zircon age distribution with that from the subducted sediments, and zircon Hf-O isotopes with those from Sumatra and Himalayas, we argue that some of the inherited zircons occurred in rocks near Toba were ultimately derived from erosion of the eastern Himalaya. Consequently, recycling of the detrital zircons together with the subducted sediments through diapirisms, followed by partial melting in the hot corner of the mantle wedge, is proposed to account for the along-arc geochemical variations of the Sunda arc volcanic rocks.

Geological background and samples. The Sunda arc is formed as a result of the subduction of the Indo-Australian plate under the Eurasian plate (Fig. 1a). The Indian oceanic crust subducts obliquely beneath Sumatra and moves towards the NNE with an average convergence rate of ~57 mm/yr[19]. The Investigator Fracture Zone on the Indian Ocean plate subducts obliquely with the same orientation beneath the Toba Caldera[20,21]. The Nicobar Fan is located offshore of northern Sumatra. It was active during the Early Miocene (~19 Ma) to Pleistocene (~1.7 Ma) and comprised predominantly of sandy and muddy turbidities, which were mainly supplied by the Ganges and Brahmaputra Rivers from the Greater Himalaya and Gangdese arc in eastern Himalaya and transported for a long distance of > 1700 km from the outlets[22,23]. Sediments from the Sunda forearc and West Burma, however, make a minor contribution to the Nicobar Fan[22].

Sumatra Island has a continental basement with a thickness of up to 39 km[24]. The tectonic development of Sumatra has been a matter of debate. It was traditionally considered to be drifted from the Gondwana during the Late Paleozoic and Mesozoic[25,26]. East Sumatra formed the southernmost part of the Sibumasu terrane, whereas West Sumatra was inferred to be derived from the Cathaysia and emplaced against the western margin of the Sibumasu terrane by dextral faulting along the Medial Sumatra Tectonic Zone (MSTZ)[25,27]. However, new detrital zircon ages from Sumatra indicate that East and West Sumatra most likely have Western Australian affinities in northern East Gondwana[28]. This is consistent with the age distribution of inherited zircons in Cenozoic sedimentary and igneous rocks of East Java, showing that the basement rocks may have Gondwana affinity[29]. Precambrian basement is not identified in the outcrops, but the occurrence of S-type granites as old as the Early Silurian indicates the existence of old metasedimentary basement rocks under Sumatra[25,30]. Tethys subduction has resulted in juvenile arc formation on Sumatra characterized by exclusively positive $\varepsilon_{Hf}(t)$ values in nearly all the magmatic and detrital zircons from the Jurassic (~200 Ma) to middle Miocene (~15 Ma)[31,32].

Our samples collected in this study include basalts and/or andesites from the Sibayak, Sipisupisu, and Sinabung volcanoes and Haranggaol Andesites near the Toba Caldera, and others slightly further to the south of the Toba Caldera along the Sunda arc on Sumatra Island (Fig. 1b). All these rocks are porphyritic in texture and contain clinopyroxene ± orthopyroxene ± olivine and plagioclase as the main phenocrysts (Supplementary Fig. 1). They belong to calc-alkaline to high-K alkaline series and slightly scatter on major element Harker diagrams (Supplementary Figs. 2, 3 and Supplementary Data 1). The exact ages of these rocks are unclear, but our new U-Pb ages of the inherited zircons imply that these rocks are formed in Quaternary (Supplementary Data 2), some even younger than the Youngest Toba Tuff (~74 ka).

Results and discussion

Along-arc geochemical variations of the Sumatran volcanic rocks. The basalts and andesites in this study have primitive mantle-normalized patterns depleted in high field strength elements (HFSE) and enriched in large ion lithophile elements (LILE), typical of arc volcanic rocks (Fig. 2). Rocks near Toba have higher rare earth element ($\sum$REE = 137–233 ppm with an average of 165 ppm) and LILE contents than those of the upper continental crust, whereas rocks away from Toba have rare earth element ($\sum$REE = 91–216 ppm with an average of 120 ppm) and LILE contents lower than those of the upper continental crust (Fig. 2). The volcanic rocks near Toba have higher $^{87}Sr/^{86}Sr$ ratios (0.70906 to 0.71377) and lower ε_{Nd} values (−10.2 to −6.57) than those away from it, which have $^{87}Sr/^{86}Sr$ (0.70469 to 0.70790) and ε_{Nd} (−4.02 to 5.27) values similar to other Sunda arc volcanic rocks (Fig. 3a–c). The basalts near Toba, in particular, have the highest $^{87}Sr/^{86}Sr$ ratios among all the terrestrial continental arc basalts reported so far (Fig. 3d). It is noteworthy that the Sr-Nd isotopes of the Sunda arc volcanic rocks in northern Sumatra exhibit systematic latitudinal variations that the $^{87}Sr/^{86}Sr$ ratios progressively increase whereas the ε_{Nd} values progressively decrease towards the Toba Caldera (Fig. 4).

Possible magma sources of the isotopically-enriched rocks near Toba include the subducting slab, mantle wedge, and overlying continental crust. The slab tear beneath Toba may facilitate asthenospheric upwelling[33–35]. However, the mafic to silicic rocks within and near the Toba Caldera do not display OIB-like trace

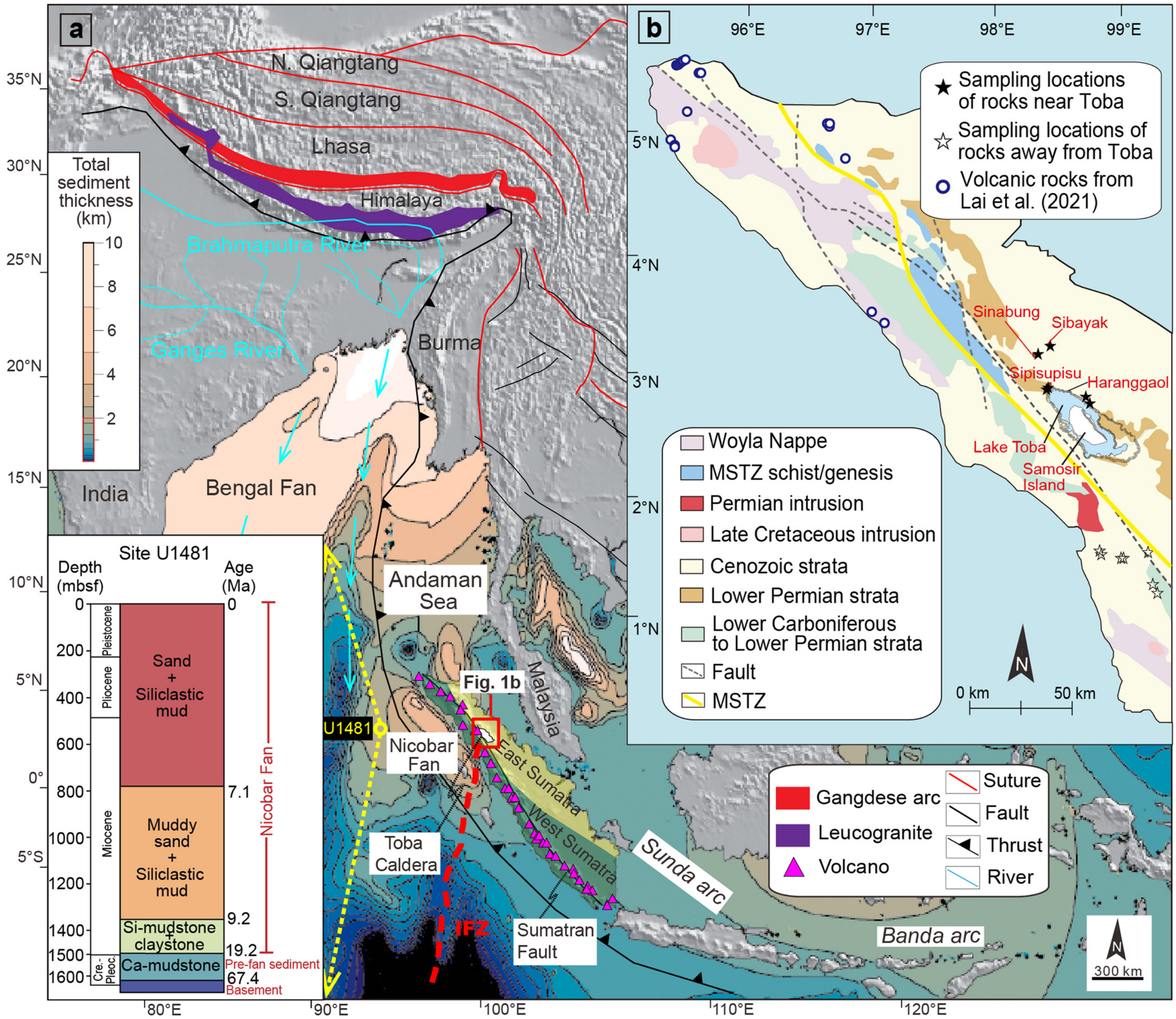

Fig. 1 Schematic geological map of the Southeast Asia and sampling locations in northern Sumatra. a Overview of the Southeast Asia. A base map of the total sediment thickness is taken from ref. [55]. Stratigraphic column of Site U1481 in the lower left corner is modified from ref. [23]. **b** A simplified geological map of northern Sumatra and the Toba Caldera. Sampling locations are marked and classified according to their distance from the Toba Caldera. IFZ-Investigator Fracture Zone, MSTZ-Medial Sumatra Tectonic Zone.

element characteristics[36], indicative of minor contributions of the upwelling Indian Ocean asthenosphere with $^{87}Sr/^{86}Sr$ ratios varying between 0.704 to 0.707[37,38] to the arc volcanic rocks near Toba. The depleted mantle-like Sr-Nd isotopic compositions of the volcanic rocks away from Toba in this study and in ref. [17] preclude the possibility that the continental lithospheric mantle beneath Sumatra is isotopically enriched. Furthermore, large amounts of fluids released from the subducting slab can alter the Sr isotopic compositions of the Sunda arc volcanic rocks but not the Nd isotopes (e.g., ref. [7]). Thus, the enriched Sr and Nd isotopic compositions of the rocks near Toba attest to substantial crustal input. One possibility is that the parental magma of the rocks near Toba was formed by crustal contamination of the depleted mantle-derived basaltic melts. Given that the Sr and Nd isotopes of the rocks near Toba do not exhibit linear correlations with whole-rock MgO and SiO_2 contents (Fig. 3a, b) and plagioclase phenocrysts from basalts near Toba do not record any signs of a primitive basaltic component from core to rim with An contents from 92 to 76 (Supplementary Fig. 4 and Supplementary Data 3), crustal contamination, if occurred, could have been early in the lower crustal magma reservoir by assimilating Sumatran lower crust. However, some of the volcanic rocks near Toba have ε_{Nd} values beyond the range of the depleted mantle and the possible basement rocks of Sumatra, as represented by the most isotopically-enriched S-type granites on Sumatra (Fig. 5a). We, therefore, infer that crustal contamination alone is unlikely to produce the Sr and Nd isotopic compositions of the rocks near Toba. The sediments on the subducting slab include those from the Nicobar Fan and the eroded Sunda forearc materials. Since the volcanic rocks on the Sunda arc, except for those near Toba, exhibit depleted mantle-like isotopic compositions[15–17], even if a large volume of the eroded Sunda arc sediments were transferred to the subarc depth, it cannot isotopically enrich the volcanic rocks near Toba. Rather, binary mixing modeling results of ε_{Nd} versus $^{87}Sr/^{86}Sr$ and ε_{Nd} versus Hf/Nd ratios show that the rocks near Toba can be produced by mixing the subducted Nicobar Fan sediments ($^{87}Sr/^{86}Sr = 0.73493$, $\varepsilon_{Nd} = -14$[6,23]) with the depleted mantle (DM, represented by N-MORB or N-MORB with minor

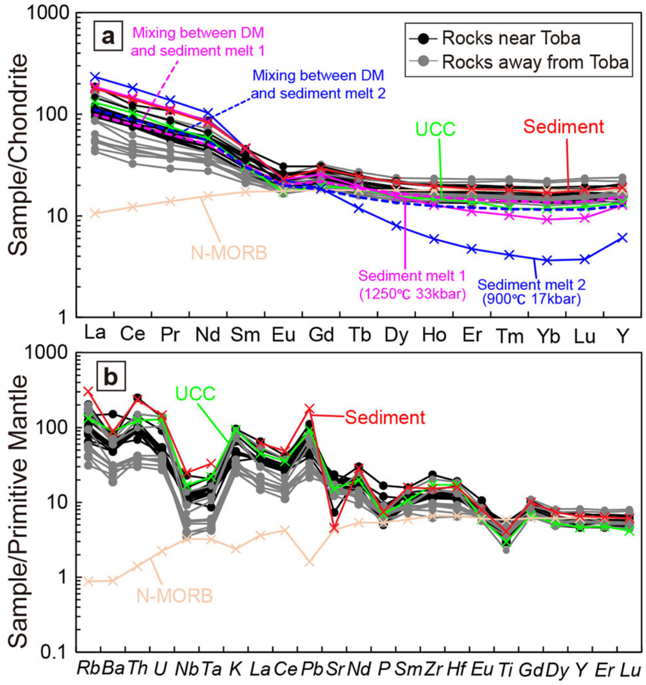

Fig. 2 Trace element characteristics of the arc volcanic rocks in northern Sumatra. a Chondrite-normalized rare earth element (REE) patterns of the studied rocks. **b** Primitive mantle-normalized trace element spider diagram of the studied rocks. Trace element and REE compositions of the N-MORB[86], upper continental crust (UCC; ref. [87]), and subducted sediments[6] are also shown for comparison. Calculated REE concentrations of the sediment melt at 1250 °C, 33 kbar (Sediment melt 1) and 900 °C, 17 kbar (Sediment melt 2) are shown in **a**. Mixing of DM (composition represented by N-MORB) with 50% sediment melt 1 and with 45 % sediment melt 2 can produce the REE patterns observed in rocks near Toba in **a**.

OIB components; Fig. 5a, b). This indicates that the primary magma of the rocks near Toba could be enriched by addition of the subducted sediments to the mantle wedge.

The rocks away from Toba, on the other hand, have trace element and Sr-Nd isotopic compositions similar to other contemporary volcanic rocks of the Sunda arc (Fig. 5a, b; refs. [39,40]). The roughly negative and scattered trends in ε_{Nd} versus SiO_2 and $^{87}Sr/^{86}Sr$ versus MgO diagrams (Fig. 3a, b), together with the binary mixing models of ε_{Nd} versus $^{87}Sr/^{86}Sr$ and ε_{Nd} versus Hf/Nd (Fig. 5) suggest that small amounts (<5%) of Sumatran crust and subducted sediments may contribute to the trace element and isotopic variations of the rocks away from Toba. This is consistent with previous U, Th, and Ra disequilibria and combined Sr-Nd-Pb isotopic and trace elemental studies suggesting that both subducted sediments and crustal contamination played important roles in generating the along-arc geochemical variations of Sunda arc lavas[15].

U-Pb-Hf-O isotopes decode the origin of the inherited zircons. Zircons were found in arc basalts and andesites both near and away from Toba (Supplementary Note 1). We filtered the zircon U-Pb age data by removing those >1500 Ma with a discordance >5% and those <1500 Ma with a discordance >10% to avoid using less concordant zircon ages to calculate their $\varepsilon_{Hf}(t)$ values (Supplementary Fig. 7; ref. [41]). Zircons in rocks near Toba have U-Pb ages spreading from <1 to ~1600 Ma, whereas those in rocks away from Toba have U-Pb ages spreading from <1 to ~900 Ma (Fig. 6b, c and Supplementary Data 2). This suggests that (1) these rocks are very young in age; and (2) these zircons are inherited from diverse crustal input. Assuming a subduction rate of 57 mm/y and a subduction length of 540 km at 190 km depth beneath Toba[19,42], a simple calculation shows that the slab below Toba now was subducted at ~9.5 Ma. This implies that zircons younger than 9.5 Ma cannot be derived from the subducted sediments. Rather, they have Hf isotopes similar to the Sumatran upper continental crust (Fig. 6b) and, therefore, could be contaminated by the shallow Sumatran crust.

To evaluate the possible sources of zircons older than 9.5 Ma, we first compare their Hf isotopes with those of the subducted sediments and Sumatran continental crust. Unfortunately, Hf isotopic data of zircons from the subducted sediments are not available. Since the sediments are predominantly sourced from the eastern Himalaya[22,23], we use Hf isotopes of detrital zircons from the Himalayas to represent those from the subducted sediments. Results show that inherited zircons older than 120 Ma from rocks near and away from Toba have indistinguishable $\varepsilon_{Hf}(t)$ values that mostly overlap with those from both Himalayas and Sumatra (Fig. 6b, c). Therefore, it is difficult to differentiate whether they come from the subducted sediments or the Sumatra crust. Nevertheless, zircons with ages of ~120 to 30 Ma from rocks near Toba display uniformly negative $\varepsilon_{Hf}(t)$ values. Rocks away from Toba do not have inherited zircons within this age range, but have inherited zircons with ages between ~20 and 15 Ma and these zircons have positive $\varepsilon_{Hf}(t)$ values (Fig. 6b). Most zircons with ages from 120 to 15 Ma on Sumatra have positive $\varepsilon_{Hf}(t)$ values due to the Meso-Tethyan subduction, through Neo-Tethyan subduction, to Indian Ocean subduction, resulting in predominant juvenile arc magmatic episodes[31]. Contemporary zircons of Himalayas, however, have both positive and negative $\varepsilon_{Hf}(t)$ values. Therefore, the negative $\varepsilon_{Hf}(t)$ values of zircons with ages between ~120 and 30 Ma from rocks near Toba indicate that they are probably derived from the subducted Nicobar Fan sediments, which possess detrital zircon grains derived from the eastern Himalaya and therefore have the same $\varepsilon_{Hf}(t)$ values with the Himalaya detrital zircons. Indeed, both the inherited zircons from rocks near Toba and the detrital zircons from the Nicobar Fan sediments have an age peak between ~55 to 40 Ma (Fig. 6a, b), indicating that some of the inherited zircons in rocks near Toba could be derived from the subducted sediments. During that period, microcontinental subduction and India-Asia collision resulted in crustal anatexis on the Himalayas, leading to the formation of S-type granitic rocks such as leucogranites, which have zircons with negative $\varepsilon_{Hf}(t)$ and high $\delta^{18}O$ values[43–45]. This could be the primary source of the Paleogene zircons with negative $\varepsilon_{Hf}(t)$ values on the Nicobar Fan. This event, however, is not known to occur on Sumatra.

Then we compare the $\delta^{18}O$ values of zircons with ages between ~55 and 40 Ma. During this time interval, the $\delta^{18}O$ values of the inherited zircons of rocks near Toba are consistently high of >9‰. Their Hf and O isotopes are comparable to those of the leucogranites in the Himalayas (Fig. 6d; refs. [21,44,46]). Consequently, we confirm that some of the inherited zircons from rocks near Toba were ultimately derived from the Himalayas. These zircons were eroded and transported by the Brahmaputra River and turbidites to the Nicobar Fan, subducted beneath northern Sumatra, and then ascended through the mantle wedge before being exposed on the surface of Sumatra. This indicates that zircon, as a resistant and refractory mineral, can survive the temperature-pressure conditions of the mantle wedge. Indeed, exotic zircons found in mantle peridotites[47,48] and Caribbean arc lavas[49,50] verify that zircon crystals can preserve in hot zircon-undersaturated environments for a considerably long period of time (tens of million years; refs. [48,51,52]).

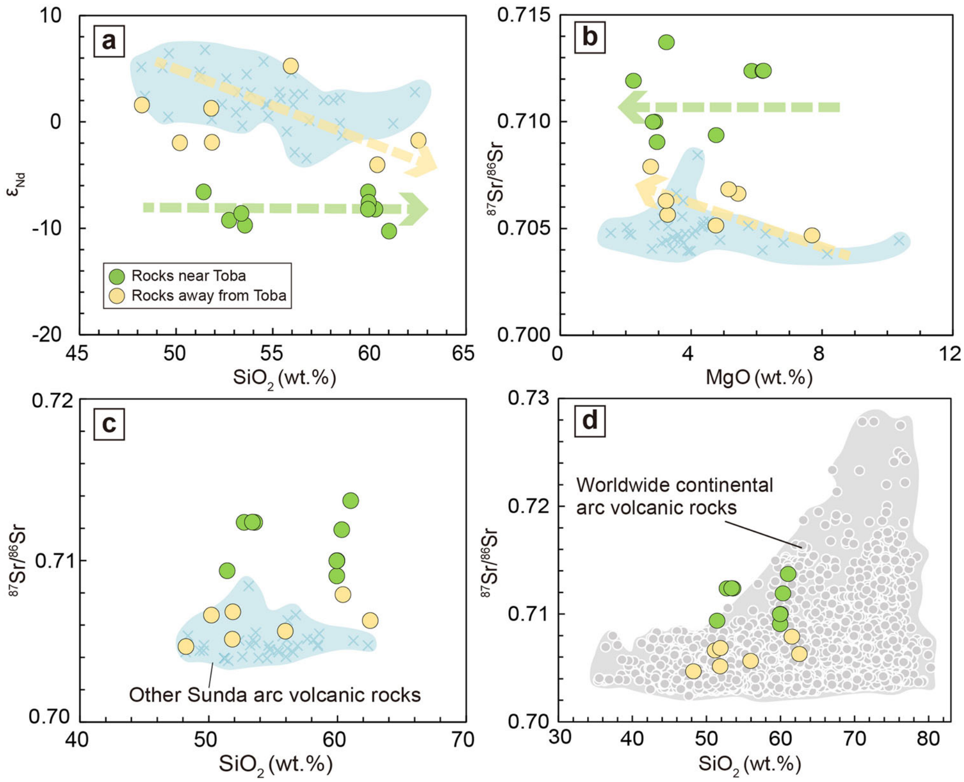

Fig. 3 Compositions of the studied volcanic rocks in northern Sumatra. a ε_{Nd} versus SiO_2 diagram displaying a roughly negative correlation for rocks away from Toba in this study and in literatures (other Sunda arc volcanic rocks[17,39,40]), whereas the ε_{Nd} ratios of rocks near Toba do not vary with increasing SiO_2 contents. **b** $^{87}Sr/^{86}Sr$ versus MgO diagram displaying a roughly negative correlation for rocks away from Toba, whereas that of rocks near Toba does not exhibit an obvious correlation. **c** $^{87}Sr/^{86}Sr$ versus SiO_2 diagram showing that the rocks near Toba have higher $^{87}Sr/^{86}Sr$ ratios than those away from Toba, which have similar $^{87}Sr/^{86}Sr$ values with other Sunda arc volcanic rocks[17,39,40]. **d** $^{87}Sr/^{86}Sr$ versus SiO_2 diagram showing that the basalts near Toba have the highest $^{87}Sr/^{86}Sr$ ratios among worldwide continental arc basalts. Compositions of worldwide continental arc volcanic rocks are from the GEOROC database (http://georoc.mpch-mainz.gwdg.de/georoc/Start.asp).

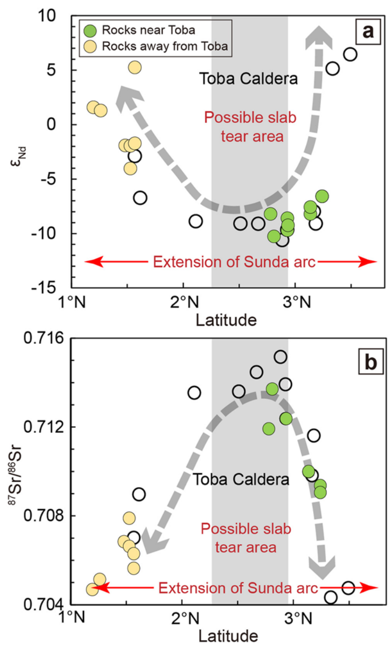

Fig. 4 Latitudinal (Along-arc) isotopic variations of Sunda arc volcanic rocks in northern Sumatra. a Variations of ε_{Nd} values with latitudes showing that arc volcanic rocks on Sumatra display decreasing ε_{Nd} values towards the Toba Caldera. **b** Similar with **a**, but for $^{87}Sr/^{86}Sr$ values. Open circles represent data from refs. [17,39] (Supplementary Data 4).

Mechanism and consequence of subduction-zone sediment recycling. Because the trace element and isotopic compositions of the subducted terrigenous sediments are similar to those of the average continental crust[3,6], it is generally difficult to distinguish the process of crustal contamination and source enrichment by sediment recycling for continental arc volcanic rocks. The Sunda trench of northern Sumatra is covered by the isotopically-enriched Nicobar Fan sediments[23]. These sediments are mainly derived from erosion of the eastern Himalaya[22,23], which exposes crustally derived leucogranites with extremely low ε_{Nd} values and high $^{87}Sr/^{86}Sr$ and $\delta^{18}O$ values (e.g., refs. [21,53]). Consequently, the relatively high ε_{Nd} values (> -10) of the Sumatran crust compared with those of the subducted sediments ($\varepsilon_{Nd} < -10$) enables us to discern the variable incorporation of the subducted sediments along the arc, which reaches a maximum in the vicinity of the Toba Caldera. The inherited zircons with ages between 60 and 40 Ma from the rocks near Toba, furthermore, have similar Hf and O isotopes with contemporary zircons from Himalayas, which also support the incorporation of subducted sediments in the formation of the mantle-derived rocks near Toba. Indeed, olivine phenocrysts from basalts near Toba have trace element contents/ratios indicating that the basalts were partial melting products of a mixed peridotite and pyroxenite mantle source (Supplementary Fig. 8), which could result from metasomatism of Si-rich sediment melts. The many young (<9.5 Ma) inherited zircons in both groups of rocks, on the other hand, indicate that shallow-level crustal contamination is a common process for Sunda arc volcanic rocks. To sum up, our study has clearly demonstrated the along-arc geochemical diversity of Sunda arc

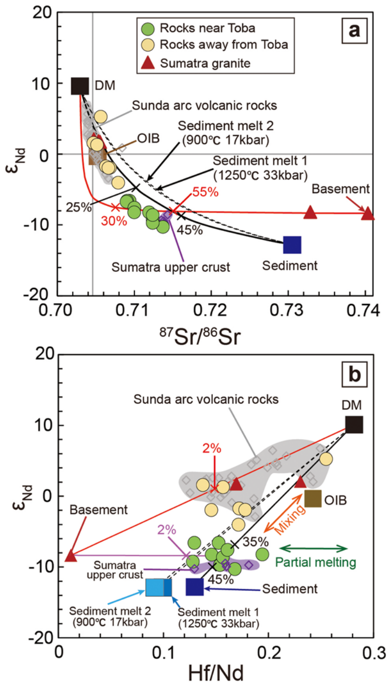

Fig. 5 Mixing diagrams between the mantle, subducted sediments, and basement rocks of Sumatra. a ε_{Nd} versus $^{87}Sr/^{86}Sr$ diagram showing that rocks near Toba can be produced by mixing of DM (represented by N-MORB[86]) with 25 to 45% sediments or sediment melts. Deviation of $^{87}Sr/^{86}Sr$ and ε_{Nd} of rocks near Toba from the modeling trends between DM and sediment melts can be explained by early extraction of Sr from the sediments by dehydration fluids. Rocks away from Toba, however, have ε_{Nd} and $^{87}Sr/^{86}Sr$ compositions that can be explained by either crustal contamination or sediment addition. Compositions of the Sumatran basements are represented by the most isotopically-enriched S-type granites on Sumatra[18]. Compositions of the previously reported Sunda arc volcanic rocks[17,39,40], which belongs to rocks away from Toba, are also plotted in the gray field. Details for the end-member compositions can be found in Supplementary Data 5. **b** ε_{Nd} versus Hf/Nd diagram indicating that rocks near Toba were probably produced by mixing of DM with 35 to 45% sediment (melts) followed by partial melting, whereas rocks away from Toba are consistent with mixing of DM with minor (<3%) Sumatra basement melts[14].

volcanic rocks that the rocks near Toba are enriched mainly due to recycling of the subducted sediments coupled with crustal contamination, whereas rocks away from Toba have predominantly undergone crustal contamination with minor sediment addition.

Our study has presented an example of sediment recycling in modern subduction zones. The inherited zircons in volcanic rocks near Toba have traveled for a long distance of ~2500 km from Himalayas, the highest mountain range (>6000 m high) on Earth, to a depth of ~150 km below sea level[20] and then rose through the hot mantle wedge (>1200 °C) to be preserved in volcanic rocks on the surface of Sumatra Island. Since the Sumatran continental crust has similar architecture across the island[24,54] and the thickness of the Nicobar Fan sediments slightly decreases from the north tip of Sumatra Island to the south (Fig. 1, ref. [55]), the spatially increasing whole-rock $^{87}Sr/^{86}Sr$ ratios towards Toba along the Sunda arc (Fig. 4) and the discovery of relict zircons derived from the subducted sediments in rocks near Toba instead of other areas indicate that sediment recycling in Sunda arc magmatism is closely associated with the unique subduction system under Toba. Coincidently, the oblique subduction of the Investigator Fracture Zone on the Indian Ocean floor is considered to propagate beneath Toba[20,21]. Seismic models show that there are two low-velocity anomaly channels connecting the subducting slab with the Toba volcano[20]. One anomaly originated from ~80 km beneath the forearc and was interpreted to result from ascent of water due to slab dehydration. The other originated from ~150 km beneath Toba and was considered to be the path of ascending fluids and melts from the slab[20].

To investigate how Nicobar Fan sediments participated in subduction-zone sediment recycling, we performed the thermodynamic modeling to obtain phase relations of the subducted Nicobar Fan sediments (composition from ref. [6]) from 10-60 kbar and 500–1300 °C using THERMOCALC version 3.45[56]. Results show that the subducted sediments do not melt on the slab surface < ~190 km (~60 kbar) in depth (Fig. 7) under the thermal and structural conditions of the Sumatran subduction zone[57]. Because the solution models used to calculate the pseudosection are calibrated for crustal pressures[56], its application to higher pressures (>2 GPa) could be problematic. In particular, the wet solidus of the sediments calculated are commonly higher than those obtained by experiments (e.g., refs. [12,58]). We argue that the pseudosection is basically reliable considering that (1) the melting reactions and residuum assemblages are consistent with the experimental results (e.g., refs. [12,58]); (2) Some experiments on fluid-present melting of meta-sediments at high pressures yield wet solidus similar to our calculations (e.g., ref. [59]), but remarkably higher than those in refs. [12,58]. Given that the experimental conditions vary in different studies and cannot be totally the same as those in the field, this could be an important factor affecting the temperature discrepancy of the wet solidus. Even if the several experimental wet solidi are taken into consideration, the P-T conditions of the slab surface subducting beneath northern Sumatra do not allow in-situ sediment melting on the slab surface (Fig. 7). Instead, the curvature of the mixing lines in ε_{Nd} versus $^{87}Sr/^{86}Sr$ diagram and the compositional distribution in ε_{Nd} versus Hf/Nd diagram of arc volcanic rocks near Toba (Fig. 5) imply that the subducted sediments could have been firstly mixed with the depleted mantle, and then undergone partial melting[14]. Transfer of the subducted sediments into the mantle wedge could occur through diapirism that the sediments rise buoyantly from the slab surface and partially melt in the hot corner of the mantle wedge[13,14,60]. According to thermodynamic modeling, dehydration melting is unlikely to occur in most sediment compositions at typical slab-top conditions and diapir formation is directly related to sediment thickness and composition, and the thermal state of the subduction zone[61]. Sediment diapir in the northern Sumatra subduction zone probably initiates at ~70 km depth with a temperature slightly higher than 500 °C[13]. According to the calculated sediment diapir trajectories[60] and the thermal structure of the Sumatran subduction zone[57], the temperature (<800 °C) of the sediment diapir trajectory from the slab surface at ~150 km depth would first increase to >1200 °C at ~100 km depth in the mantle wedge and then decrease to <800 °C at Moho[60]. Melting of sediment diapirs started from the surface inwards and may not obtain equilibrium under P-T conditions above the sediments' liquidus[60,61]. As such, the subducted Nicobar Fan sediments, which have undergone dehydration and eclogitization, would partially melt during ascent (Fig. 7).

Numerical modeling indicates that sediment diapirs ascending through the mantle wedge beneath the volcanic arc would undergo less than ~40–50% total melting[60,61]. Because (1) the relict mineral phases and their proportions change along the P-T path of the sediment diapir trajectory, (2) melt and the relict mineral phases may not achieve equilibrium at each depth (temperature), and (3) mantle metasomatism occurs during ascending of the Si-rich sediment melts, the compositions of the

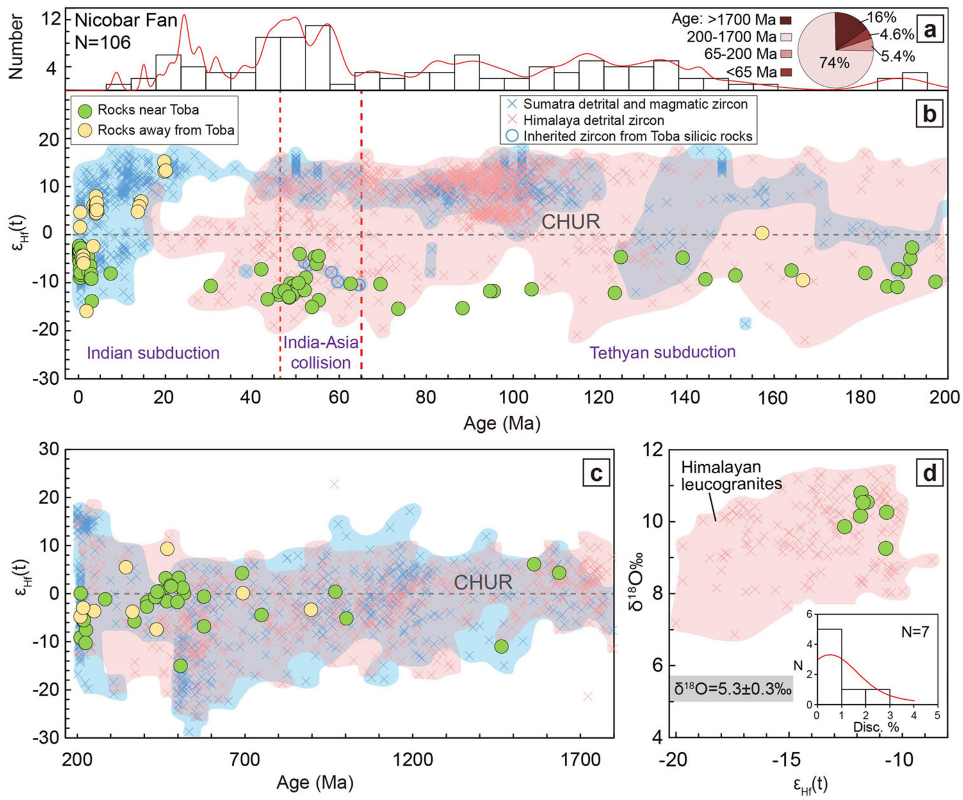

Fig. 6 Zircon U-Pb ages and Hf-O isotopic compositions of the studied rocks compared with those from the subducted Nicobar Fan sediments, Sumatra Island, and Himalayas. a Detrital zircon age spectra of the Nicobar Fan sediments (data from ref. [22]). Inset is a pie graph showing the proportions of detrital zircons from the Nicobar Fan sediments with different age ranges. **b** Zircon ages (<200 Ma) versus $\varepsilon_{Hf}(t)$ values of the studied samples, also shown are ages versus $\varepsilon_{Hf}(t)$ values of detrital zircons from Himalayas[88–92] and detrital and magmatic zircons from Sumatra[28,32,93]. **c** Similar with b but for ages >200 Ma. **d** $\delta^{18}O$ versus $\varepsilon_{Hf}(t)$ values of inherited zircons with ages varying between 30 and 55 Ma from rocks near Toba. Pink crosses represent $\varepsilon_{Hf}(t)$ and $\delta^{18}O$ values of contemporary zircons from Himalaya leucogranites[46]. The insert shows the U-Pb age discordance for zircons used in **d**. CHUR-Chondritic Uniform Reservoir.

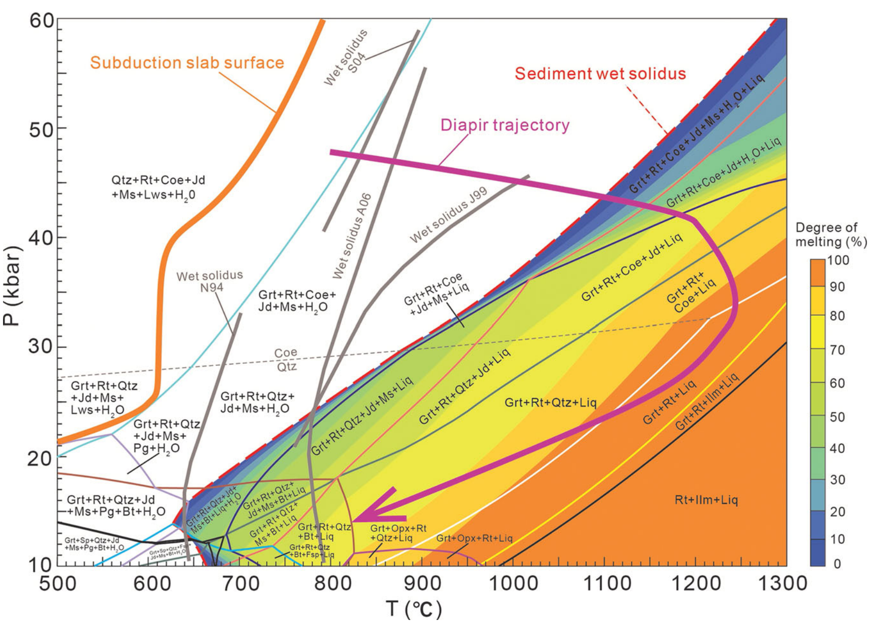

Fig. 7 P-T diagram showing the phase relations of the subducted Nicobar Fan sediments and possible diapir trajectory of the sediments. P-T conditions of the slab surface is from ref. [57]. The diapir trajectory is cited from ref. [60]. The gray lines represent the experimentally determined wet solidi of metapelite and metagreywacke: N94 from ref. [10], J99 from ref. [59], S04 from ref. [58], and A06 from ref. [94]. The P-T pseudosections are shaded with a warmer color tone as the partial melting degrees increase. Bt-Biotite, Coe-Coesite, Grt-Garnet, Fsp-Feldspar, Ilm-Ilmenite, Jd-Jadeite, Liq-Liquid, Lws-Lawsonite, Ms-Muscovite, Opx-Orthopyroxene, Pg-Paragonite, Qtz-Quartz, Rt-Rutile, Sp-Sphene.

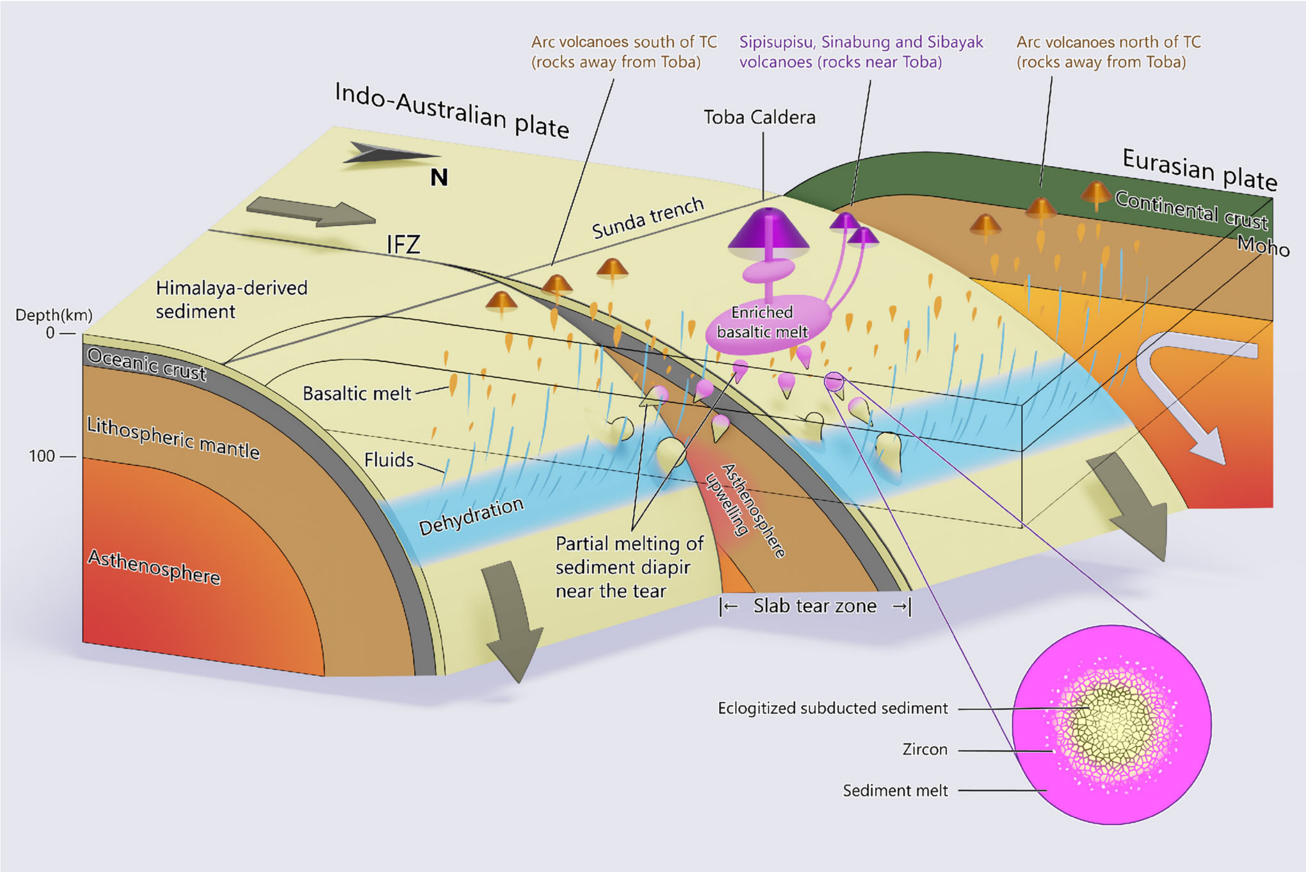

Fig. 8 3D scenograph illustrating the model of Indian Ocean floor subduction and sediment diapirs under northern Sumatra. Oblique subduction of the Investigator Fracture Zone (IFZ) resulted in a slab tear beneath the Toba Caldera (TC). The subducted sediments at ~150 km depth around the slab tear area have undergone diapirism followed by partial melting within the hot corner of the mantle wedge, which generated geochemically enriched arc volcanic rocks with inherited zircons from the sediments in the vicinity of the Toba Caldera (rocks near Toba). Farther away from the IFZ, dehydration of the subducting plate and flux melting of the mantle wedge were the dominant processes responsible for the depleted mantle-like Sr and Nd isotopes of the rocks away from Toba. A zoom-in view of sediment melting with some undissolved zircon grains is shown in the bottom right corner.

sediment melts added to the arc volcanic rocks near Toba are difficult to calculate. The best solution is to model the rare earth element contents of the sediment melts at two end-member conditions: 900 °C, 17 kbar and 1250 °C, 33 kbar using proportions of relict mineral phases and their partition coefficients (Fig. 7 and Supplementary Note 2, ref. [62]). Due to the existence of garnet as a relict mineral phase, subarc sediment melts commonly have large Dy/Yb fractionation (Fig. 2a). Calculation shows that ~45 and 50% of the sediment melts are needed under conditions of 900 °C, 17 kbar and 1250 °C, 33 kbar, respectively, to mix with the depleted mantle (represented by N-MORB) to generate the most primitive basalts of rocks near Toba (Fig. 2a and Supplementary Table 1). These values might be an overestimation considering that (1) the light rare earth elements can be elevated by aqueous fluids during dehydration[7] and by early fractionation of olivine ± pyroxenes ± plagioclase; (2) some extent of REE enrichment can be induced by reaction of the fluid-fluxed melts with the initially depleted mantle wedge peridotites. Indeed, this proportion is higher than that derived from the two end-member modeling results in ε_{Nd} versus $^{87}Sr/^{86}Sr$ and ε_{Nd} versus Hf/Nd diagrams, which indicates that ~30 to 45% of the sediment melts are needed to produce the geochemical characteristics of the rocks near Toba. This scenario also coincides with the geophysical evidence showing that the depth of the deep low-velocity anomaly does not extend to the slab surface but about 50 km above it[20], which may imply that the sediment diapirs start to melt after ascending ~50 km above the slab surface (Fig. 8). In addition, numerical simulations indicate that the diapirs would melt from the surface inward, and the maximum melting proportions commonly do not exceed 40–50%[60]. If this is true, this may indicate that a considerable amount of the subducted sediments is relaminated at the base of the Sumatran lower crust.

Given that the Toba silicic rocks also have inherited zircons of ~60 to 40 Ma with similar $\varepsilon_{Hf}(t)$ values to those from basalts and andesites near Toba (Fig. 6b), we infer that Toba silicic rocks with evolved Sr and Nd isotopic compositions[36] could also be sourced from an enriched mantle hybridized by the subducted sediments. This study further indicates that zircons can be used to trace crustal recycling in subduction zones, which can not only occur between mantle and crust, but also between separate continental blocks. The latitudinal trace element and isotopic variations of volcanic rocks along the Sunda arc imply that the increasing amount of sediment melting associated with diapirism could have been related to the thermal upwelling through the slab tear beneath Toba (Fig. 8). Therefore, the geometry of the subducted plate, to some extent, controls the geochemical diversity of arc volcanic rocks[63–65], which is also evidenced by the Northern and Southern Cordillera continental arc and the Lesser Antilles island arc volcanic rocks[66–68].

Methods

Whole-rock major and trace element compositions. Whole-rock major element compositions of the samples were analyzed using X-ray fluorescence spectroscopy

(Rigaku RIX-2000) at the Department of Geosciences, National Taiwan University, with analytical uncertainties of <5%. Loss-on-ignition (LOI) was determined by heating samples at 950 °C for 60 min and recording the percentage of weight loss. Whole-rock trace element concentrations were determined by inductively coupled plasma-mass spectrometry (ICP-MS) using an Agilent 7500cx spectrometer at the Institute of Earth Sciences, Academia Sinica, following the procedures described in ref. [69]. The USGS standards AGV-2, BHVO-2, and BCR-2 were analyzed together as reference materials. Analytical precisions for most trace elements were better than 3%.

Whole-rock Sr-Nd isotopes. Whole-rock $^{87}Sr/^{86}Sr$ and $^{143}Nd/^{144}Nd$ values were determined by a Nu Plasma II MC-ICP-MS (multiple collector-inductively coupled plasma-mass spectrometer) at the Institute of Earth Sciences, Academia Sinica. The mass fractionation for $^{87}Sr/^{86}Sr$ and $^{143}Nd/^{144}Nd$ ratios were normalized against $^{86}Sr/^{88}Sr = 0.1194$ and $^{146}Nd/^{144}Nd = 0.7219$, respectively. The mean $^{87}Sr/^{86}Sr$ ratio of NBS SRM 987 standard during data acquisition was 0.710308 ± 14 ($n = 9$) and the mean $^{143}Nd/^{144}Nd$ ratio of Etsu JNdi-1 standard was 0.512108 ± 6 ($n = 6$). The 2σ analytical errors are commonly <0.000015 for $^{87}Sr/^{86}Sr$ and <0.000008 for $^{143}Nd/^{144}Nd$ for routine analyses of individual unknown samples. Detailed analytical protocols can be referred to ref. [70].

Zircon U-Pb age and Hf-O isotopic analyses. Zircons were separated from rock samples using standard density and magnetic separation techniques. Measurements of U, Th, and Pb isotopes in zircons were conducted using CAMECA IMS-1280HR at the Institute of Geology and Geophysics, Chinese Academy of Sciences (IGG-CAS). The O^{2-} primary ion beam was accelerated at ~13 kV, with an intensity of ~10 nA. The aperture illumination mode (Kohler illumination) was used to produce an elliptical spot of about 20 × 30 μm in size. Pb/U and Th/U ratios were determined relative to the standard zircon Plešovice[70], analyses of which were interspersed with those of unknown grains. Zircons older than 2 Ma were analyzed following routine procedures[71], whereas those younger than 2 Ma were dated on the condition of ^{238}U-^{230}Th disequilibrium as those described by ref. [72].

Zircon oxygen isotopic analyses were performed using CAMECA IMS-1280. Measured $^{18}O/^{16}O$ ratios were normalized to the Vienna Standard Mean Ocean Water (VSMOW) compositions ($^{18}O/^{16}O = 0.0020052$). The measured oxygen isotopic data were corrected for instrumental mass fractionation (IMF) using the Penglai zircon standard ($\delta^{18}O_{VSMOW} = 5.3$ ‰; ref. [73]). The internal precision of each analysis was better than 0.3 ‰ (2σ standard error). The external precision evaluated by the reproducibility of repeated analyses of the Qinghu zircon was 0.38 ‰ (2 SD). Repeated measurements of the Qinghu zircon standard during the analytical session yielded weighted mean $\delta^{18}O$ of 5.46 ± 0.40 ‰ (2 SD), consistent with the reported value of 5.4 ± 0.2 ‰ (2 SD)[74].

In situ zircon Hf isotopic analyses were carried out on the same spot previously analyzed for U-Pb-O isotopes using a New Wave UP 213 LA microprobe attached to a Nu Plasma HR multi-collector ICP-MS system at the Institute of Earth Sciences, Academia Sinica. The ablation spot was 50 μm in diameter and the ablation rate was 8 Hz. The standard zircon Mud Tank was analyzed to monitor the instrumental conditions. It yielded an average $^{176}Hf/^{177}Hf$ ratio of 0.282490 ± 24 (2 SD), in agreement with the recommended value[75]. Plešovice, 91500 and TEMORA zircons served as the secondary external reference materials for data quality control. They have average $^{176}Hf/^{177}Hf$ values of 0.282483 ± 21 (2 SD), 0.282314 ± 23 (2 SD), and 0.282689 ± 30 (2 SD), respectively, in accordance with literature values reported in refs. [76,77]. Measured $^{176}Hf/^{177}Hf$ and $^{176}Lu/^{177}Hf$ ratios were used to calculate initial $^{176}Hf/^{177}Hf$ ratios, using a ^{176}Lu decay constant of 1.865 ± 10^{-11} year^{-1} (ref. [78]). The present-day $^{176}Hf/^{177}Hf = 0.282772$ and $^{176}Lu/^{177}Hf = 0.0332$ of chondrite[79] were adopted to calculate $\varepsilon_{Hf}(t)$ values.

Plagioclase major element and $^{87}Sr/^{86}Sr$ isotopic analysis. Major elements of plagioclase were analyzed using a JEOL JXA-8230 microprobe at the Key Laboratory of Orogenic Belts and Crustal Evolution, School of Earth and Space Sciences, Peking University. The analysis was carried out using a beam current of 10 nA, an accelerating voltage of 15 kV, and a beam size of 1–2 μm. Typical analytical uncertainties for all the elements were better than 1.5%.

$^{87}Sr/^{86}Sr$ ratios of plagioclase were measured using a Nu Plasma II MC-ICP-MS at the School of Earth and Space Sciences, Peking University. An ArF excimer laser ablation system of Geolas HD (193 nm) was used. The samples were ablated at a repetition rate of 5 Hz and an energy density of 10 J/cm^2 with a 90-μm spot size for 40 s. The analytical accuracy was evaluated by repeated analyses of three apatite standards of Slyudyanka, Mud Tank, and Otter Lake. The average $^{87}Sr/^{86}Sr$ ratios of the standards were 0.70805 ± 21 (2 SD; 26 analyses) for Slyudyanka, 0.70311 ± 13 (2 SD; 21 analyses) for Mud Tank and 0.70442 ± 17 (2 SD; 20 analyses) for Otter Lake, which agreed well with the standard values obtained by solution MC-ICP-MS analyses[80].

Phase equilibria modeling. Phase equilibria modeling was performed using THERMOCALC 3.45[56] with dataset ds62[81], in a model system Na_2O-CaO-K_2O-FeO-MgO-Al_2O_3-SiO_2-H_2O-TiO_2-Fe_2O_3 (NCKFMASHTO). Mineral activity-composition relationships adopted were liquid (i.e., silicate melt)[82], garnet[82], orthopyroxene[82], biotite[82], muscovite[82] and paragonite[82]; feldspars[83]; ilmenite[84]; jadeite[85]; and quartz, coesite, rutile, sphene, and lawsonite (pure phases). The fluid phase was assumed to be H_2O. The water content (8.18 wt%) of the subducted sediments was cited from ref. [6]. The Fe^{3+}/Fe_T ratio was assumed to be ~0.05, which was close to the QFM buffer. The bulk compositions of the sediments from the trench of northern Sumatra[6] used for calculations were normalized to molar proportions in the NCKFMASHTO system (Table 1).

Table 1 Molar proportions of the subducted sediments for thermodynamic modeling.

H_2O	SiO_2	Al_2O_3	CaO	MgO	FeO_T	K_2O	Na_2O	TiO_2	O
24.31	53.51	7.29	3.20	3.30	3.92	1.50	2.17	0.43	0.1

Data availability

The dataset used in this study are available at https://doi.org/10.6084/m9.figshare.21258261 (last access: 02 October 2022).

Received: 28 December 2021; Accepted: 2 November 2022;
Published online: 17 November 2022

References

1. Plank, T. & Langmuir, C. H. Tracing trace elements from sediment input to volcanic output at subduction zones. *Nature* **362**, 739–743 (1993).
2. Chan, L.-H. & Kastner, M. Lithium isotopic compositions of pore fluids and sediments in the Costa Rica subduction zone: implications for fluid processes and sediment contribution to the arc volcanoes. *Earth Planet. Sci. Lett.* **183**, 275–290 (2000).
3. Stern, R. J. Subduction zones. *Rev. Geophys.* **40**, 3-1-3–38 (2002).
4. Morris, J. D. & Ryan, J. G. Subduction zone processes and implications for changing composition of the upper and lower mantle. *Treatise Geochem.* **2**, 568 (2003).
5. Zheng, Y.-F. Subduction zone geochemistry. *Geosci. Front.* **10**, 1223–1254 (2019).
6. Plank, T. *The Chemical Composition of Subducting Sediments* (Elsevier, 2014).
7. Kessel, R., Schmidt, M. W., Ulmer, P. & Pettke, T. Trace element signature of subduction-zone fluids, melts and supercritical liquids at 120–180 km depth. *Nature* **437**, 724–727 (2005).
8. Kimura, J.-I. Modeling chemical geodynamics of subduction zones using the Arc Basalt Simulator version 5. *Geosphere* **13**, 992–1025 (2017).
9. Li, H., Hermann, J. & Zhang, L. Melting of subducted slab dictates trace element recycling in global arcs. *Sci. Adv.* **8**, eabh2166 (2022).
10. Nichols, G. T., Wyllie, P. J. & Stern, C. R. Subduction zone melting of pelagic sediments constrained by melting experiments. *Nature* **371**, 785–788 (1994).
11. Hall, P. S. & Kincaid, C. Diapiric flow at subduction zones: a recipe for rapid transport. *Science* **292**, 2472–2475 (2001).
12. Hermann, J. & Spandler, C. J. Sediment melts at sub-arc depths: an experimental study. *J. Petrol.* **49**, 717–740 (2008).
13. Behn, M. D., Kelemen, P. B., Hirth, G., Hacker, B. R. & Massonne, H.-J. Diapirs as the source of the sediment signature in arc lavas. *Nat. Geosci.* **4**, 641–646 (2011).
14. Nielsen, S. G. & Marschall, H. R. Geochemical evidence for mélange melting in global arcs. *Sci. Adv.* **3**, e1602402 (2017).
15. Turner, S. & Foden, J. U, Th and Ra disequilibria, Sr, Nd and Pb isotope and trace element variations in Sunda arc lavas: predominance of a subducted sediment component. *Contrib. Mineral. Petrol.* **142**, 43–57 (2001).
16. Mucek, A. E. et al. Post-supereruption recovery at Toba Caldera. *Nat. Commun.* **8**, 15248 (2017).
17. Lai, Y.-M. et al. Mid-Miocene volcanic migration in the westernmost Sunda arc induced by India-Eurasia collision. *Geology* **49**, 713–717 (2021).
18. Gasparon, M. & Varne, R. Sumatran granitoids and their relationship to Southeast Asian terranes. *Tectonophysics* **251**, 277–299 (1995).
19. Natawidjaja, D. H. et al. Paleogeodetic records of seismic and aseismic subduction from central Sumatran microatolls, Indonesia. *J. Geophys. Res.* **109**, B04306 (2004).
20. Koulakov, I. et al. The feeder system of the Toba supervolcano from the slab to the shallow reservoir. *Nat. Commun.* **7**, 12228 (2016).
21. Liu, S., Suardi, I., Yang, D., Wei, S. & Tong, P. Teleseismic traveltime tomography of Northern Sumatra. *Geophys. Res. Lett.* **45**, 13,231–13,239 (2018).

22. McNeill, L. C. et al. Understanding Himalayan erosion and the significance of the Nicobar Fan. *Earth Planet. Sci. Lett.* **475**, 134–142 (2017).
23. Chen, W.-H. et al. Drainage evolution and exhumation history of the eastern Himalaya: Insights from the Nicobar Fan, northeastern Indian Ocean. *Earth Planet. Sci. Lett.* **548**, 116472 (2020).
24. Sakaguchi, K., Gilbert, H. & Zandt, G. Converted wave imaging of the Toba Caldera, Indonesia. *Geophys. Res. Lett.* **33**, (2006).
25. Metcalfe, I. *Gondwana Dispersion and Asian Accretion* (Taylor & Francis, 1999).
26. Barber, A. J., Crow, M. J. & Milsom, J. S. Sumatra: geology, resources and tectonic evolution. *Geol. Soc. Mem.* **31**, (2005).
27. Barber, A. J. & Crow, M. J. An evaluation of plate tectonic models for the development of Sumatra. *Gondwana Res.* **6**, 1–28 (2003).
28. Zhang, X. et al. Detrital zircons dismember Sibumasu in East Gondwana. *J. Geophys. Res.* **123**, 6098–6110 (2018).
29. Smyth, H. R., Hamilton, P. J., Hall, R. & Kinny, P. D. The deep crust beneath island arcs: Inherited zircons reveal a Gondwana continental fragment beneath East Java, Indonesia. *Earth Planet. Sci. Lett.* **258**, 269–282 (2007).
30. Xu, C. et al. Geochronological and geochemical characteristics of early Silurian S-type granitic gneiss in Takengon area of Northern Sumatra and its tectonic implications. *Earth Science* **45**, 2077–2090 (2020).
31. Zhang, X. et al. A 6000-km-long Neo-Tethyan arc system with coherent magmatic flare-ups and lulls in South Asia. *Geology* **47**, 573–576 (2019).
32. Li, S. et al. Mesozoic juvenile crustal formation in the easternmost Tethys: zircon Hf isotopic evidence from Sumatran granitoids, Indonesia. *Geology* **48**, 1002–1005 (2020).
33. Rosenbaum, G., Gasparon, M., Lucente, F. P., Peccerillo, A. & Miller, M. S. Kinematics of slab tear faults during subduction segmentation and implications for Italian magmatism. *Tectonics* **27**, (2008).
34. Cocchi, L., Passaro, S., Tontini, F. C. & Ventura, G. Volcanism in slab tear faults is larger than in island-arcs and back-arcs. *Nat. Commun.* **8**, 1451 (2017).
35. Kong, F., Gao, S. S., Liu, K. H., Ding, W. & Li, J. Slab dehydration and mantle upwelling in the vicinity of the Sumatra subduction zone: evidence from receiver function imaging of mantle transition zone discontinuities. *J. Geophys. Res.***125**, e2020JB019381 (2020).
36. Chesner, C. A. Petrogenesis of the Toba Tuffs, Sumatra, Indonesia. *J. Petrol.* **39**, 42 (1998).
37. Dupré, B. & Allègre, C. J. Pb–Sr isotope variation in Indian Ocean basalts and mixing phenomena. *Nature* **303**, 142–146 (1983).
38. Hamelin, B., Dupré, B. & Allègre, C. J. Pb-Sr-Nd isotopic data of Indian Ocean ridges: new evidence of large-scale mapping of mantle heterogeneities. *Earth Planet. Sci. Lett.* **76**, 288–298 (1986).
39. Gasparon, M. *Origin and Evolution of Mafic Volcanics of Sumatra (Indonesia): Their Mantle Sources, and The Roles of Subducted Oceanic Sediments and Crustal Contamination*. Doctoral thesis, University of Tasmania (1993).
40. Luhr, J. F. & Haldar, D. Barren island volcano (NE Indian Ocean): island-arc high-alumina basalts produced by troctolite contamination. *J. Volcanol. Geotherm. Res.* **149**, 177–212 (2006).
41. Guitreau, M. & Blichert-Toft, J. Implications of discordant U–Pb ages on Hf isotope studies of detrital zircons. *Chem. Geol.* **385**, 17–25 (2014).
42. Lange, D. et al. The fine structure of the subducted investigator fracture zone in western Sumatra as seen by local seismicity. *Earth Planet. Sci. Lett.* **298**, 47–56 (2010).
43. Xia, Q.-X. et al. The origin of garnets in anatectic rocks from the Eastern Himalayan syntaxis, Southeastern Tibet: constraints from major and trace element zoning and phase equilibrium relationships. *J. Petrol* **60**, 2241–2280 (2019).
44. Wu, F.-Y. et al. Highly fractionated Himalayan leucogranites and associated rare-metal mineralization. *Lithos* **352–353**, 105319 (2020).
45. Yang, Z. et al. Microcontinent subduction and S-type volcanism prior to India–Asia collision. *Sci. Rep.* **11**, 14882 (2021).
46. Hopkinson, T. N. et al. The identification and significance of pure sediment-derived granites. *Earth Planet. Sci. Lett.* **467**, 57–63 (2017).
47. Song, S. et al. Geochronology of diamond-bearing zircons from garnet peridotite in the North Qaidam UHPM belt, Northern Tibetan Plateau: a record of complex histories from oceanic lithosphere subduction to continental collision. *Earth Planet. Sci. Lett.* **234**, 99–118 (2005).
48. Liu, Y. et al. Continental and oceanic crust recycling-induced melt–peridotite interactions in the trans-North China Orogen: U–Pb dating, Hf isotopes and trace elements in zircons from mantle xenoliths. *J. Petrol.* **51**, 537–571 (2010).
49. Rojas-Agramonte, Y. et al. Recycling and transport of continental material through the mantle wedge above subduction zones: a Caribbean example. *Earth Planet. Sci. Lett.* **436**, 93–107 (2016).
50. Torró, L. et al. Recycling in the subduction factory: Archaean to Permian zircons in the oceanic Cretaceous Caribbean island-arc (Hispaniola). *Gondwana Res* **54**, 23–37 (2018).
51. Siebel, W. et al. Prolonged mantle residence of zircon xenocrysts from the western Eger rift. *Nat. Geosci.* **2**, 886–890 (2009).
52. Xu, Z., Zheng, Y.-F. & Zhao, Z.-F. Zircon evidence for incorporation of terrigenous sediments into the magma source of continental basalts. *Sci. Rep.* **8**, 178 (2018).
53. Deniel, C., Vidal, P., Fernandez, A., Le Fort, P. & Peucat, J.-J. Isotopic study of the Manaslu granite (Himalaya, Nepal): inferences on the age and source of Himalayan leucogranites. *Contr. Mineral. Petrol.* **96**, 78–92 (1987).
54. Seismology, G. et al. Sharpening the tomographic image of the subducting slab below Sumatra, the Andaman Islands and Burma. *Geophys. J. Int.* **182**, 433–453 (2010).
55. Straume, E. et al. GlobSed: updated total sediment thickness in the World's Oceans. *Geochem. Geophys. Geosyst.* **20**, 1756–1772 (2019).
56. Powell, R. & Holland, T. J. B. An internally consistent dataset with uncertainties and correlations: 3. Applications to geobarometry, worked examples and a computer program. *J. Metamorph. Geol.* **6**, 173–204 (1988).
57. Hippchen, S. & Hyndman, R. D. Thermal and structural models of the Sumatra subduction zone: Implications for the megathrust seismogenic zone. *J. Geophys. Res.* **113**, (2008).
58. Schmidt, M. W., Vielzeuf, D. & Auzanneau, E. Melting and dissolution of subducting crust at high pressures: the key role of white mica. *Earth Planet. Sci. Lett.* **228**, 65–84 (2004).
59. Johnson, M. C. & Plank, T. Dehydration and melting experiments constrain the fate of subducted sediments. *Geochem. Geophys. Geosyst.* **1**, (1999).
60. Zhang, N., Behn, M. D., Parmentier, E. M. & Kincaid, C. Melt segregation and depletion during ascent of buoyant diapirs in subduction zones. *J. Geophys. Res.* **125**, e2019JB018203 (2020).
61. Klein, B. Z. & Behn, M. D. On the evolution and fate of sediment diapirs in subduction zones. *Geochem. Geophys. Geosyst.* **22**, e2021GC009873 (2021).
62. Bédard, J. H. A catalytic delamination-driven model for coupled genesis of Archaean crust and sub-continental lithospheric mantle. *Geochim. Cosmochim. Acta* **70**, 1188–1214 (2006).
63. Levin, V., Shapiro, N., Park, J. & Ritzwoller, M. Seismic evidence for catastrophic slab loss beneath Kamchatka. *Nature* **418**, 763–767 (2002).
64. Tang, G.-J. et al. Asthenosphere-lithosphere interaction triggered by a slab window during ridge subduction: trace element and Sr-Nd-Hf-Os isotopic evidence from Late Carboniferous tholeiites in the western Junggar area (NW China). *Earth Planet. Sci. Lett.* **329**, 84–96 (2012).
65. Menant, A., Sternai, P., Jolivet, L., Guillou-Frottier, L. & Gerya, T. 3D numerical modeling of mantle flow, crustal dynamics and magma genesis associated with slab roll-back and tearing: the eastern Mediterranean case. *Earth Planet. Sci. Lett.* **442**, 93–107 (2016).
66. Davidson, J. P. Lesser Antilles isotopic evidence of the role of subducted sediment in island arc magma genesis. *Nature* **306**, 253–256 (1983).
67. Thorkelson, D. J., Madsen, J. K. & Sluggett, C. L. Mantle flow through the Northern Cordilleran slab window revealed by volcanic geochemistry. *Geology* **39**, 267–270 (2011).
68. Rosenbaum, G., Sandiford, M., Caulfield, J. & Garrison, J. M. A trapdoor mechanism for slab tearing and melt generation in the northern Andes. *Geology* **47**, 23–26 (2018).
69. Lin, I.-J. et al. Geochemical and Sr–Nd isotopic characteristics of Cretaceous to Paleocene granitoids and volcanic rocks, SE Tibet: Petrogenesis and tectonic implications. *J. Asian Earth Sci* **53**, 131–150 (2012).
70. Lee, H.-Y. et al. Geochemical and Sr–Nd isotopic constraints on the genesis of the Cenozoic Linzizong volcanic successions, southern Tibet. *J. Asian Earth Sci* **53**, 96–114 (2012).
71. Li, X.-H., Liu, Y., Li, Q.-L., Guo, C.-H. & Chamberlain, K. R. Precise determination of Phanerozoic zircon Pb/Pb age by multicollector SIMS without external standardization. *Geochem. Geophys. Geosyst.* **10**, (2009).
72. Huang, Y.-S. et al. 238 U– 206 Pb dating of U-series disequilibrium zircons by secondary ion mass spectrometry. *J. Anal. At. Spectrom.* **36**, 999–1006 (2021).
73. Li, X.-H. et al. Penglai zircon megacrysts: a potential new working reference material for microbeam determination of Hf–O isotopes and U–Pb age. *Geostand. Geoanal. Res.* **34**, 117–134 (2010).
74. Li, X. et al. Qinghu zircon: a working reference for microbeam analysis of U-Pb age and Hf and O isotopes. *Chin. Sci. Bull.* **58**, 4647–4654 (2013).
75. Woodhead, J. & Hergt, J. A preliminary appraisal of seven natural zircon reference materials for in situ Hf isotope determination. *Geostand. Geoanal. Res.* **29**, 183–195 (2007).
76. Sláma, J. et al. Plešovice zircon — A new natural reference material for U–Pb and Hf isotopic microanalysis. *Chem. Geol.* **249**, 1–35 (2008).
77. Wu, F.-Y., Yang, Y.-H., Xie, L.-W., Yang, J.-H. & Xu, P. Hf isotopic compositions of the standard zircons and baddeleyites used in U–Pb geochronology. *Chem. Geol.* **234**, 105–126 (2006).
78. Scherer, E., Munker, C. & Mezger, K. Calibration of the lutetium-hafnium clock. *Science* **293**, 683–687 (2001).
79. Blichert-Toft, J. & Albarède, F. The Lu-Hf isotope geochemistry of chondrites and the evolution of the mantle-crust system. *Earth Planet. Sci. Lett.* **148**, 243–258 (1997).
80. Yang, Y.-H. et al. Sr and Nd isotopic compositions of apatite reference materials used in U–Th–Pb geochronology. *Chem. Geol.* **385**, 35–55 (2014).

81. Holland, T. J. B. & Powell, R. An improved and extended internally consistent thermodynamic dataset for phases of petrological interest, involving a new equation of state for solids. *J. Metamorph. Geol.* **29**, 333–383 (2011).
82. White, R. W., Powell, R., Holland, T. J. B., Johnson, T. E. & Green, E. C. R. New mineral activity–composition relations for thermodynamic calculations in metapelitic systems. *J. Metamorph. Geol.* **32**, 261–286 (2014).
83. Holland, T. & Powell, R. Activity–composition relations for phases in petrological calculations: an asymmetric multicomponent formulation. *Contrib. Mineral. Petrol.* **145**, 492–501 (2003).
84. White, Powell & Holland, Worley The effect of TiO_2 and Fe_2O_3 on metapelitic assemblages at greenschist and amphibolite facies conditions: mineral equilibria calculations in the system $K_2O–FeO–MgO–Al_2O_3–SiO_2–H_2O–TiO_2–Fe_2O_3$. *J. Metamorph. Geol.* **18**, 497–511 (2000).
85. Green, E. C. R. et al. Activity–composition relations for the calculation of partial melting equilibria in metabasic rocks. *J. Metamorph. Geol.* **34**, 845–869 (2016).
86. Sun, S.-S. & McDonough, W. F. Chemical and isotopic systematics of oceanic basalts: implications for mantle composition and processes. *Geol. Soc. Spec. Publ.* **42**, 313–345 (1989).
87. Rudnick, R. L. & Gao, S. Composition of the Continental Crust. in *Treatise on Geochemistry*, 2nd edition, vol. 4, 1–51 (Elsevier, Amsterdam, 2014).
88. Liang, Y.-H. et al. Detrital zircon evidence from Burma for reorganization of the eastern Himalayan river system. *Am. J. Sci.* **308**, 618–638 (2008).
89. Hu, X., Sinclair, H. D., Wang, J., Jiang, H. & Wu, F. Late Cretaceous-Palaeogene stratigraphic and basin evolution in the Zhepure Mountain of southern Tibet: implications for the timing of India-Asia initial collision. *Basin Res* **24**, 520–543 (2012).
90. Robinson, R. A. J. et al. Large rivers and orogens: the evolution of the Yarlung Tsangpo–Irrawaddy system and the eastern Himalayan syntaxis. *Gondwana Res.* **26**, 112–121 (2014).
91. Wang, J.-G., Wu, F.-Y., Tan, X.-C. & Liu, C.-Z. Magmatic evolution of the Western Myanmar Arc documented by U–Pb and Hf isotopes in detrital zircon. *Tectonophysics* **612–613**, 97–105 (2014).
92. Vadlamani, R., Wu, F.-Y. & Ji, W.-Q. Detrital zircon U–Pb age and Hf isotopic composition from foreland sediments of the Assam Basin, NE India: constraints on sediment provenance and tectonics of the Eastern Himalaya. *J. Asian Earth Sci.* **111**, 254–267 (2015).
93. Hsu, C. C. *Detrital Zircon U–Pb and Hf Isotopic Study in Northwestern Sumatra, Indonesia*. Master thesis, National Taiwan University (2016).
94. Auzanneau, E., Vielzeuf, D. & Schmidt, M. W. Experimental evidence of decompression melting during exhumation of subducted continental crust. *Contrib. Mineral. Petrol.* **152**, 125–148 (2006).

Acknowledgements

We thank Prof. Sayed Murtadha from Syiah Kuala University, Indonesia, for his long-term collaboration, which includes providing logistic help with the fieldwork and sample export. We thank Dr. Guibin Zhang, Ms. Jiao Li, Xiaoxiao Ling, Hongxia Ma, and Nan Li for their help with lab work and Drs. Xiaochi Liu and Ming Tang for constructive discussions. We thank Mr. Mingkang Yang for his help with the 3D scenograph. Detailed and constructive comments from the editor and three reviewers are greatly appreciated. This study is supported by the National Science Foundation of China (grant 41872058).

Author contributions

P.-P.L. designed the research. X.H.L., Q.L.L., and H.-Y.L. helped with the data acquisition. B.W. performed the phase equilibria modeling. P.-P.L. and M.-H.G. wrote the manuscript. P.-P.L., M.-H.G., S.-L.C., X.-H.L., and W.T. contributed ideas to the interpretation of results or manuscript revisions.

Competing interests

The authors declare no competing interests.

Additional information

Supplementary information The online version contains supplementary material available at https://doi.org/10.1038/s43247-022-00611-6.

Correspondence and requests for materials should be addressed to Ping-Ping Liu.

Peer review information *Communications Earth & Environment* thanks the anonymous reviewers for their contribution to the peer review of this work. Primary Handling Editors: João Duarte, Joe Aslin.